Journal of Engineering Science and Technology Review 17 (4) (2024) 171-180

Research Article

JOURNAL OF
Engineering Science and Technology Review

www.jestr.org

Lane Keeping Assistance for Electric Power Steering Systems based on the Robust Sliding Mode Observer

Songzhuo Shi[1] and Guangda Chen[*]

[1]*School of Electrical and Information Engineering, Beihua University, Jilin 132013, China*

Received 23 May 2024; Accepted 27 August 2024

Abstract

Lane-keeping assistance (LKA) systems aim to address the vehicle deviation problem from normal lanes due to driver distraction, and their performance is affected by factors such as the stability of the steering system and external interference. This study proposed a vehicle LKA strategy based on the electric power steering system (EPS) to reveal the relationship between the control strategy and the performance of LKA systems. Firstly, an EPS system, a vehicle three-degree-of-freedom dynamics model, and a driver model were established for the nonlinear electromechanically coupled vehicle EPS system. Both the serial lane-keeping control strategy for the EPS system controller based on robust sliding mode observers and the model prediction controller based on vehicle trajectory were devised. Then, based on various driving conditions, the vehicle's intervention coefficient outputs were dynamically adjusted in accordance with the lateral safety deviation and the driver's manual force. Finally, the intervention coefficients of the lane-keeping system were designed, and the accuracy of the control strategy was verified through experiments. Results show that after adding lane-keeping auxiliary control, the wheel turning angle is reduced by a maximum of 9° , the traverse angular velocity is decreased by a maximum of 0.52 rad, and the vehicle lateral offset is reduced by a maximum of 3.4 m. This study provides a significant reference for constructing vehicle models and evaluating the performance of LKA control strategies.

Keywords: Lane keeping, Electric power steering system, Sliding mode control, Vehicle trajectory model prediction

1. Introduction

The Lane-keeping assistance (LKA) system is currently one of the most typical active safety driving assistance technologies; its function is to help the driver keep the vehicle in the lane and prevent it from deviating due to distractions to the driver [1]. The application demand for LKA systems is gradually increasing, and the related technical research has also made remarkable progress. Increasing units are involved in the study, design, production, and application of LKA systems [2]. The static output feedback control method improves the maneuvering stability of the LKA control system to a certain extent [3].

Lane-keeping control strategies with high efficiency, flexibility, and safety have become research hotspots to effectively address the demands for high control accuracy and maneuvering stability of LKA systems [4,5]. With the application of LKA systems in vehicles, the study of related technology has made remarkable progress [6-8]. However, the complexity of vehicle driving conditions introduces considerable challenges to lane-keeping control strategies.

Scholars have conducted numerous studies of the performance and control effects of different control strategies and parameter settings of LKA systems [9-12]. However, studies on the robustness of the control strategy of the LKA system and the intervention timing under complex road conditions were few. With the increasing complexity of vehicle driving conditions, the existing LKA system is mainly designed for simple driving scenarios and cannot accurately determine or handle complex road conditions. The existing LKA system is mainly based on the detection of vehicle positions and lane lines. With a limited understanding of the driver's intention, this system cannot accurately determine whether the driver wants to deviate from the lane, resulting in miscalculations and conflicts. Therefore, realizing the high reliability of the control strategy of LKA systems and human-vehicle coordination control and achieving high maneuvering stability is of considerable engineering importance.

To this end, this study designed a driver-in-the-loop model prediction controller based on vehicle trajectory and a robust sliding-mode observer based on a serial LKA control strategy by establishing a vehicle electric power steering system model. The fuzzy control algorithm was used to design intervention coefficients, and the intervention of the LKA system on the driver was reduced, expecting to enhance the poor maneuvering stability of human-vehicle interaction in the LKA system. The study results provide a reference for the application development and optimization of LKA system control strategies.

The remainder of this study is organized as follows. Section 2 gives the relevant background, including a statement of the LKA system problem. Section 3 establishes a model of the entire vehicle EPS system, the vehicle, and the driver and designs the LKA control strategy and the LKA system intervention coefficients. Section 4 uses the model to analyze the performance of the LKA system, and finally, the conclusions are summarized in Section 5.

2. State of the art

Road traffic problems have become increasingly serious in recent years. The survey by the US Highway Traffic Safety

*E-mail address: sisongzhuo@126.com
ISSN: 1791-2377
doi:10.25103/jestr.174.19

Administration shows that 37% of traffic fatalities are caused by lane departure [13]. Electric power steering (EPS) is a product of automotive electronic control technology, according to the concepts of energy savings and environmental protection [14]. When lane departure occurs, the EPS system provides an auxiliary torque to return the vehicle to the intended lane, which has become a research hotspot in the field of lane keeping. Guo designed an LKA system, where the LKA torque was superimposed with the EPS torque and output via the booster motor of the EPS system. The intervention and exit strategies of the LKA system were designed, but the intervention parameters were not optimized [15]. Kővári applied Monte Carlo tree search to efficiently select the most suitable reinforcement learning model for training by simulating prediction reward quality and avoiding comprehensive training. Resource consumption decreased, but the control strategy disregarded the actual driving conditions of vehicles [16]. Huang designed a fuzzy control-based coordinated control method for lane keeping by using an electric power steering system as the actuator of LKA systems and realized steering deviation correction by controlling the electric motor [17]. Instead of the camera sensor based on reinforcement learning for lane-keeping systems, Kim used the information of the surrounding objects obtained by the LiDAR sensor, which verified the reliability of the LiDAR sensor data in real environments [18]. Munadi took an automatic guided vehicle equipped with a navigation system as a research object and used computer vision and fuzzy logic control as a LKA system control strategy. The practical effect of the lane-keeping control strategy with different light intensities was studied, but only the effect of light was considered in the control strategy [19].

Zheng designed a real-time lane departure warning system based on the improved Sobel algorithm and Hough transform to identify lane lines, and lane departure warning was realized through the matching degree with the warning decision module; however, the prediction of lane trajectory change was not used as a warning parameter [20]. Alex designed a centralized and decentralized LKA system based on a linear parameter varying (LPV) system, H∞, and sliding mode algorithms and incorporated driver behavior into the decision-making layer. However, the system was not designed with driver intervention parameters [21]. Marumo et al. investigated the effects of multi-articulated vehicle stability control on the performance of an LKA system and evaluated the control effect by checking computer simulation with a driver-vehicle system [22]. Chouki proposed a new shared control concept for intelligent LKA systems [23]. Tang et al. designed a robust model predictive control algorithm based on linear matrix inequality for lane-keeping tracking control of commercial vehicles, which transformed the model predictive control problem into a min-max optimization problem using linear matrix inequality; however, the lane paths were homogeneous [24]. With vehicle lateral position and traverse angle as control quantities, Illés designed a lane-assisted holding system and ensured the accuracy of the control quantity using the PID control algorithm. However, the synergy between the driver and the lane-keeping system was not considered in the control strategy [25]. Zhan et al. designed an activation strategy for LKA systems for commercial vehicles based on a single-point pre-scanning model and proportional-differential control algorithm, proposed a humanoid driving steering model, and controlled the power-assisted motor to realize the lane keeping function [26]. Maryam applied the vehicle longitudinal dynamics model predictive control strategy to LKA systems, using vehicle longitudinal speed as the control parameter [27].Chen et al. proposed a preview lane-keeping control method monitored by a safety barrier and designed a safety protection controller to improve the computational efficiency of online solving and guarantee the bounded error [28]. Tan et al. introduced a fuzzy control-based lane keeping algorithm that avoided the influence of the variation of dynamic parameters in the vehicle dynamics model on the stability of the system [29].

The above studies discussed the design of the control strategy of LKA systems under different working conditions and the timing of driver intervention. On the one hand, the existing studies have numerous uncertainties in the design of LKA control strategies under the nonlinear and complex electromechanical coupling characteristics of the EPS system. Studies on the strategy under multi-working conditions are limited. On the other hand, the study of the timing of driver intervention in LKA systems is scarce. This study established a model of the entire vehicle EPS system and the controller of the LKA system. Based on the characteristics of the control strategy, the influence of the LKA system on the stability of the vehicle handling under different working conditions was comprehensively discussed, and the driver intervention coefficients were designed, expecting to provide strong support for optimizing the control strategy of LKA systems. Meanwhile, the effectiveness and superiority of the proposed control strategy were verified through simulation and comparative analysis to establish a solid foundation for the practical application and promotion of the lane-keeping technology.

3. Methodology

3.1 Modeling of the EPS steering system

The EPS system is regarded as a simple rigid body, and the dynamics model is established according to the mass point dynamics theory of classical Newtonian mechanics theory and the dynamics theory of rigid body plane motion, as shown in Fig. 1. This system comprises the following three parts: steering wheel and upper input steering shaft, power-assisted motor and steering transmission. The dynamic equations of the system are established in accordance with Fig. 1:

The automotive mechanical steering system comprises multiple moment transfer paths, including rotational inertia, damping moment, friction moment, and clearance. The steering input column is modeled as equation (1):

$$J_s\ddot{\theta}_s + B_s\theta_s + K_s(\theta_s - \theta_e) = T_d \tag{1}$$

where J_s is the equivalent moment of inertia of the steering input shaft and steering wheel, K_s is the stiffness coefficient of the torsion bar of the torque transducer, B_s is the damping coefficient of the steering input shaft, θ_s is the steering wheel angle of rotation, θ_e is the steering output shaft angle of rotation, and T_d is the input torque of the steering wheel.

The torque expression of the torque sensor is shown in equation (2):

$$T_s = K_s(\theta_s - \theta_e) \tag{2}$$

where T_s is the output torque of the torque sensor.

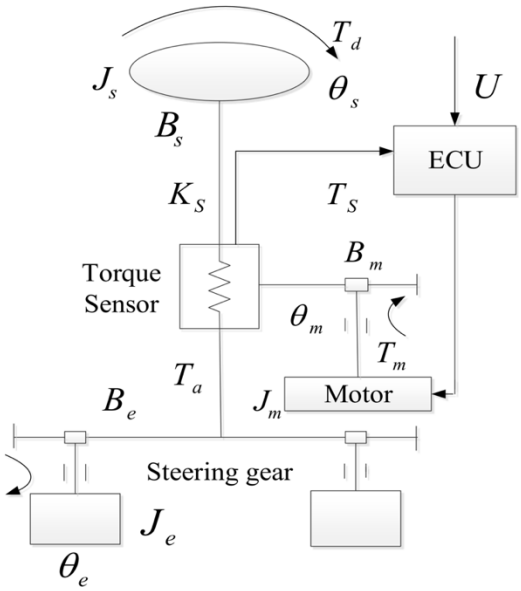

Fig. 1. Dynamical model of EPS system

The steering column input moment is converted into a horizontal force by the rack and pinion, and the kinetic expression is shown as equation (3):

$$m_s\ddot{x}_r + b_s\dot{x}_r + K_s x_r = \frac{T_w}{r_p} - F_\delta \tag{3}$$

where m_r is the steering cross tie mass, b_r is the rack damping coefficient, K_r is the stiffness coefficient of the spring, x_r is the rack displacement, T_w is the reaction torque acting on the steering output shaft, r_p is the pinion radius, and F_δ is the road surface force.

Under steering power assistance, the output torque of the motor is transmitted to the steering column after decelerating and increasing the torque through the worm gear reduction mechanism, and the kinetic model of the power-assisted motor is established considering the inertia, friction, and damping, as respectively shown in equations (4) and (5):

$$J_m\ddot{\theta}_m + B_m\dot{\theta}_m + K_m(\theta_m - G\theta_e) = T_m \tag{4}$$

$$U = Ri + L\dot{i} + K_c\dot{\theta}_m \tag{5}$$

where J_m is the motor rotational inertia, B_m is the motor viscous friction coefficient, θ_m is the motor rotational angle, K_m is the equivalent stiffness coefficient of the motor and the reduction mechanism, T_m is the motor output torque, U is the motor terminal voltage, R is the motor armature resistance, L is the motor armature inductance, i is the motor current, and K_c is the motor counter electromotive force constant.

The deceleration mechanism is the motor's deceleration and torsion increasing mechanism and its dynamic model is shown in equation (6):

$$J_e\ddot{\theta}_e + B_e\dot{\theta}_e = K_s(\theta_s - \theta_e) + K_m G(\theta_m - G\theta_e) - T_w \tag{6}$$

where J_e is the rotational inertia of the reduction mechanism, B_e is the damping coefficient of the reduction mechanism, and G is the reduction ratio of the worm gear reducer.

The expression for the relationship between the boost torque of the motor and the angular transmission ratio of the gearhead is shown in equation (7):

$$T_a = K_m G(\theta_m - G\theta_e) \tag{7}$$

where T_a is the boost torque output by the motor.

The model expression for the force on the rack and pinion connected cross ties is shown as equation (8):

$$F_r = K_r x_r \tag{8}$$

where F_r is the force received by the steering tie rod when the steering is applied.

The steering wheel input to the rack and pinion output of Fr is approximated as a rigid shaft connection, and the conversion relationship is shown as equation (9):

$$\theta_p = \frac{x_r}{r_p} \tag{9}$$

where θ_p is the pinion angle.

Therefore, the angle of the steering pinion is similar to the output angle of the column and the converted angle of the rack displacement, obtaining equations (10) and (11), respectively:

$$J_s\ddot{\theta}_s + B_s\dot{\theta}_s + K_s(\theta_s - \theta_p) = T_d \tag{10}$$

$$J_m\ddot{\theta}_m + B_m\dot{\theta}_m + K_m(\theta_m - G\theta_p) = T_m \tag{11}$$

Based on the above equations, the complete dynamic model expression of the EPS system can be obtained, as shown in equations (12) and (13):

$$J_e\frac{\ddot{x}_r}{r_p^2} + m_r\ddot{x}_r + B_e\frac{\dot{x}_r}{r_p^2} + b_r\dot{x}_r + K_r x_r = \frac{K_s}{r_p}(\theta_s - \theta_p) + \frac{GK_m}{r_p}(\theta_m - G\theta_p) - F_\delta \tag{12}$$

$$J_e\frac{\ddot{x}_r}{r_p^2} + m_r\ddot{x}_r + B_e\frac{\dot{x}_r}{r_p^2} + b_r\dot{x}_r + F_r = \frac{K_s}{r_p}(\theta_s - \theta_p) + \frac{GK_m}{r_p}(\theta_m - G\theta_p) - F_\delta \tag{13}$$

The motor reduction mechanism and the rack pinion are simplified into a model as shown in equation (14):

$$M_r = \frac{J_e}{r_p^2} + m_r \tag{14}$$

where M_r is the equivalent mass of the reduction mechanism and pinion rack.

The reduction mechanism and the rack and pinion damping coefficients are simplified into a model as shown in equation (15):

$$B_r = \frac{B_e}{r_p^2} + b_r \tag{15}$$

where B_r is the equivalent damping coefficient of the reduction mechanism and pinion rack.

The model after equivalence is shown in equation (16):

$$\begin{aligned} &m_r\ddot{x}_r + B_r\dot{x}_r + F_r = \frac{K_s}{r_p}(\theta_s - \theta_p) + \\ &\frac{GK_m}{r_p}(\theta_m - G\theta_p) - F_\delta \end{aligned} \tag{16}$$

Equations (1)–(16) are converted into the system state control equation. The system state variable is $x = \left[\theta_s \quad \dot{\theta}_s \quad x_r \quad \dot{x}_r \quad \theta_m \quad \dot{\theta}_m \quad i\right]$; the input variable is $u = \left[T_d \quad U \quad T_w\right]^T$; the output variable is $y = \left[T_a \; i \; T_s \; \theta_s \; \ddot{\theta}_m\right]$; and the system state equation is expressed as shown in equation (17):

$$\begin{aligned} \dot{x} &= Ax + Bu \\ y &= Cx + Du \end{aligned} \tag{17}$$

3.2 Three-degree-of-freedom vehicle model

The three-degree-of-freedom model indicates the following: the degree of freedom of the vehicle for translational movement along the y-axis is characterized by the velocity; the degree of freedom of rotation around the z-axis is characterized by the angular velocity of the transverse pendulum; and the degree of freedom of rotation around the x-axis is characterized by the angle of the lateral deflection. The kinetic equations are established as equation (18):

$$\begin{aligned} &M(\dot{v} + rV) + M_s h\ddot{f} = Y_b b + Y_r r + \\ &Y_f f + Y_d d \\ &I_z\dot{r} - I_{xz}\ddot{f} = N_b b + N_r r + N_f f + \\ &N_d d + N_p P \\ &I_{sx}\ddot{f} - I_{xz}\dot{r} + M_s h(\dot{v} + rV) = L_f f + \\ &L_p\dot{f} \end{aligned} \tag{18}$$

where M is the vehicle mass; v is the lateral velocity; r is the yaw velocity; V is the longitudinal velocity; M_s is the suspension mass; h is the distance from the center of gravity of suspension mass to roll axis; f is the roll angle; Y_b is the ground lateral reaction force caused by unit vehicle sideslip angle; b is the side deflection angle of center of mass; Y_r is the lateral ground reaction force caused by unit vehicle yaw rate; Y_f is the ground lateral reaction force caused by unit vehicle roll angle; Y_d is the ground lateral reaction force caused by unit vehicle front-wheel angle; d is the front-wheel angle; I_z is the inertia around the vertical axis; I_{xz} is the inertia product of the mass of the vehicle on the x- and z-axes; N_b is the moment on the z-axis generated by the lateral deflection angle of the center of mass per unit of mass; N_r is the moment on the z-axis generated by the angular velocity of the transverse pendulum per unit of mass; N_f is the moment on the z-axis generated by the angular velocity of the sideways tilt per unit of mass; and N_d is the moment on the z-axis generated by the angular velocity of the front wheel per unit of mass. N_p is the moment to the z-axis generated by unit front-wheel angle; p is the sideways tilt angular velocity; I_{sz} is the rotational moment of inertia of the suspended mass to the x-axis; L_f is the external moment to the x-axis generated by unit sideways tilt angular velocity; and L_p is the external moment to the x-axis generated by sideways tilt angular velocity.

3.3 Driver model

Fig. 2 shows the vehicle trajectory with constant transverse angular velocity, where point M is the center of mass position at the current moment, point L is the pre-sighting point on the target trajectory, and Δf is the pre-sighting deviation. As shown in this figure, the lateral deviation of point C is obtained as equation (19):

$$y_{CG} = \tan(\frac{\theta}{2} + \beta)x_{CG} \tag{19}$$

where θ is the center angle of the circle, and β is the sideslip angle of the center of mass.

After t_p, the ideal center of mass of the vehicle is located at point M (coinciding with point C). Uniform circular motion is assumed due to the substantially smaller v than V, as shown in equation (20):

$$y_{CG} = \Delta f, \theta = \omega t_p, \mathrm{x}_{CG} \approx Vt_p \tag{20}$$

The ideal yaw velocity ω_r is shown in equation (21):

$$\omega_r = 2[\arctan(\frac{\Delta f}{Vt_p}) - \beta]t_p^{-1} \tag{21}$$

Equation (22) is the ideal front-wheel angle:

$$\delta = 2L[\arctan(\frac{\Delta f}{Vt_p}) - \beta](1 + KV^2)(t_p V)^{-1} \tag{22}$$

3.4 Model predictive controller design based on vehicle trajectory

In assisted driving conditions, according to the vehicle state and real-time parameters, such as velocity, yaw angle, lateral offset, steering wheel torque, and steering wheel angle, the road condition and maneuvering information of the driver collected by the camera on the vehicle is taken as the input of the controller. Prioritizing the decision making of the driver, assisted by the lane keeping system, man-machine synergistic control is studied. LKA torque is superimposed to ensure the basic assisting force of the EPS system.

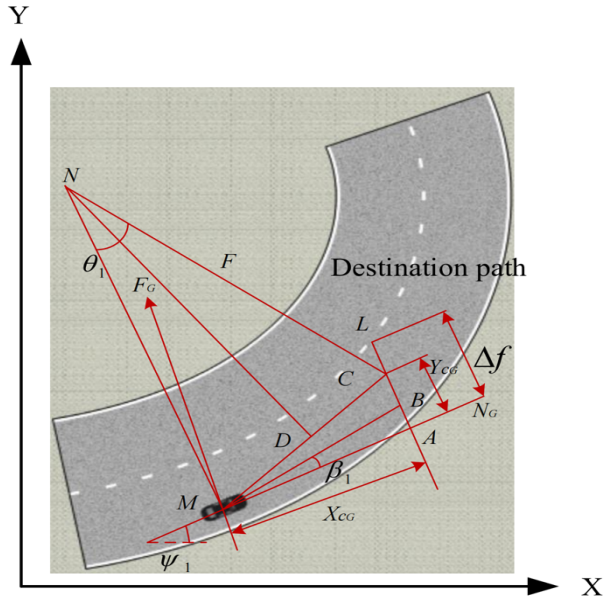

Fig. 2. Vehicle trajectory with constant yaw velocity

A model prediction controller based on the vehicle's trajectory is used to calculate the target rotating angle. A controller based on a high-gain sliding mode observer is designed to obtain the target assisting torque for the target assisting torque and the torque input applied by the driver. Meanwhile, considering the state of the driver and the vehicle, the intervention coefficient is introduced to ensure a smooth transition between the driver maneuvering and LKA states. With the manual force of the driver and the motion state of the vehicle as input variables and the intervention coefficient as the output variable, the fuzzy control method is used to control the steering motor to actively correct the traveling direction of the vehicle. Fig. 3 shows the block diagram of the lane-keeping control system.

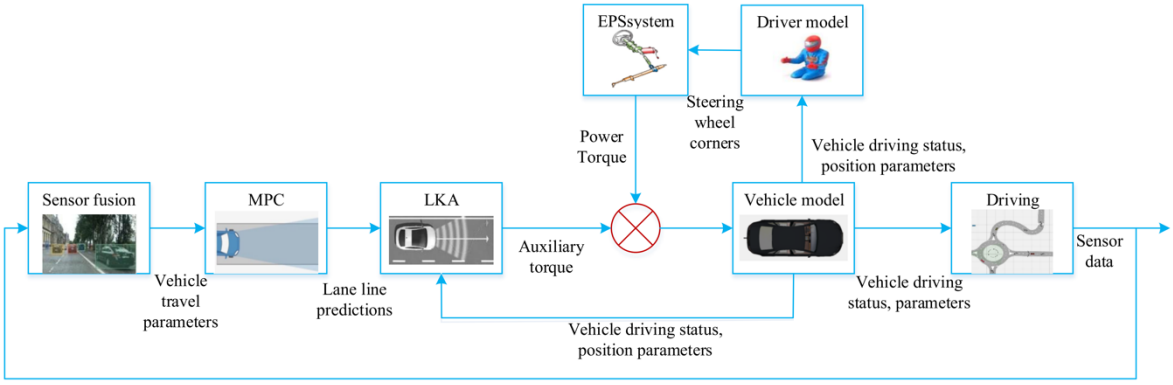

Fig. 3. Block diagram of lane-keeping control system

Model predictive control based on vehicle trajectory is used to predict the vehicle trajectory according to the inputs and states of the vehicle.

The expression for vehicle kinematics is presented in equation (23):

$$E\dot{x}=A(x)+Bu \tag{23}$$

$$x=[\beta \quad r \quad \phi \quad \mu]^T$$

$$E=\begin{bmatrix} MV & 0 & 0 & M_s h \\ 0 & I_z & 0 & -I_{xz} \\ M_s hV & -I_{xz} & 0 & sI_x \\ 0 & 0 & 1 & 0 \end{bmatrix}$$

$$A=\begin{bmatrix} Y_b & Y_r - MV & Y_f & 0 \\ N_b & N_r & N_f & N_p \\ 0 & -M_s hV & L_f & L_p \\ 0 & 0 & 0 & 1 \end{bmatrix}$$

$$B=[Y_d \quad N_d \quad 0 \quad 0]^T$$

where u is the input quantity, and x is the status quantity.

A description of the motion trajectory of the reference vehicle is available for a given reference trajectory, and each point on the motion trajectory satisfies the above kinematic equations, with r representing the reference quantity. The general form is shown as equation (24):

$$\dot{x}_r=f(x_r,u_r) \tag{24}$$

where $x_r=[\beta_r \quad r_r \quad \phi_r \quad \mu_r]^T$, $u_r=\dot{\phi}$.

Expanding equation (24) at the reference trajectory point using Taylor series and neglecting higher order terms:

$$\dot{x}=f(x_r,u_r)+\frac{\partial f(x,u)}{\partial x}\Big|_{\substack{x=x_r \\ u=u_r}}(x_r-x)+\frac{\partial f(x,u)}{\partial u}\Big|_{\substack{x=x_r \\ u=u_r}}(u-u_r) \tag{25}$$

The linearized vehicle error model is obtained by subtracting equation (24) from equation (25). The linearized vehicle error model is discretized to use the model for model prediction controller design.

$$\tilde{\chi}(k+1)=A_{k,t}\tilde{\chi}(k)+B_{k,t}\tilde{u}(k) \tag{26}$$

The objective function is shown as equation (27):

$$J(k)=\sum_{i=1}^{N_p}\left\|\Delta\eta(k+i\,|\,t)\right\|^2+\sum_{i=1}^{N_m}\left\|\Delta u(k+i\,|\,t)\right\|^2 \tag{27}$$

Equation (26) is converted based on equation (28):

$$\xi(\mathrm{k}\,|\,\mathrm{t})=\begin{bmatrix}\tilde{\chi}(k\,|\,t)\\ \tilde{\mathrm{u}}(k-1\,|\,t)\end{bmatrix} \tag{28}$$

The new state space expression is obtained as equation (29):

$$\begin{aligned}\xi(k+1\,|\,t)&=\tilde{A}_{k,t}\xi(k\,|\,t)+\tilde{B}_{k,t}\Delta u(k\,|\,t)\\ \eta(k\,|\,t)&=\tilde{C}_{k,t}\xi(k\,|\,t)\end{aligned} \tag{29}$$

The predicted output expression (30) of the system is derived as follows:

$$Y(t)=\Psi_t\xi(t\,|\,t)+\Theta_t\Delta u(\mathrm{t}) \tag{30}$$

$$Y(\mathrm{t})=\begin{bmatrix}\eta(t+1\,|\,t)\\ \eta(t+2\,|\,t)\\ \vdots\\ \eta(t+N_p\,|\,t)\end{bmatrix}$$

$$\Psi_t=\begin{bmatrix}\tilde{C}_{t,t}\tilde{A}_{t,t}\\ \tilde{C}_{t,t}\tilde{A}_{t,t}^2\\ \vdots\\ \tilde{C}_{t,t}\tilde{A}_{t,t}^{N_p}\end{bmatrix}$$

$$\Theta_t=\begin{bmatrix}\tilde{C}_{t,t}\tilde{B}_{t,t} & 0 & 0 & 0\\ \tilde{C}_{t,t}\tilde{A}_{t,t}\tilde{B}_{t,t} & \tilde{C}_{t,t}\tilde{B}_{t,t} & 0 & 0\\ \vdots & & & \vdots\\ \tilde{C}_{t,t}\tilde{A}_{t,t}^{N_m}\tilde{B}_{t,t} & \tilde{C}_{t,t}\tilde{A}^{N_m-1}\tilde{B}_{t,t} & 0 & 0\\ \vdots & & & \vdots\\ \tilde{C}_{t,t}\tilde{A}^{N_p-1}\tilde{B}_{t,t} & \tilde{C}_{t,t}\tilde{A}^{N_p-2}\tilde{B}_{t,t} & 0 & 0\end{bmatrix}$$

$$\Delta u(t)=\begin{bmatrix}\Delta u(t\,|\,t)\\ \Delta u(t+1\,|\,t)\\ \vdots\\ \Delta u(t+N_m\,|\,t)\end{bmatrix}$$

where the control variable expression is as follows:

$$u_{min}(t+k)\le u(t+k)\le u_{max}(t+k)$$

The control incremental constraint expression is as follows:

$$\Delta u_{min}(t+k)\le\Delta u(t+k)\le\Delta u_{max}(t+k)$$

where u_{min} and u_{max} are the minimum and maximum values of the front-wheel angle, respectively; Δu_{min} and Δu_{max} are the minimum and maximum values of the control increment, respectively.

3.5 Design of EPS system controller based on robust sliding-mode observer

According to the state equation of the EPS system shown in equation (17), θ_s, r, θ_m and i are selected as the state variables. Considering the modeling uncertainty and external disturbance moment, equation (17) is simplified as shown below:

$$\begin{aligned}\ddot{\theta}_s&=-\frac{k_s}{J_s}\theta_s-\frac{k_s}{J_s}\dot{\theta}_s+\frac{k_s}{rJ_s}+\frac{1}{J_s}T_d\\ \ddot{r}&=\frac{k_s}{rm_r}\theta_s-\frac{k_s+k_mG^2}{r^2m_r}r-\frac{b_r}{m_r}\dot{r}+\frac{k_mG}{rm_r}\theta_m-\frac{1}{m_r}T_w\\ \ddot{\theta}_m&=\frac{k_mG}{rJ_m}r-\frac{k_m}{J_m}\theta_m-\frac{b_m}{J_m}\dot{\theta}_m\\ \dot{i}&=-\frac{k_f}{L}\dot{\theta}_m-\frac{R}{L}i+\frac{1}{L}U_s+\Delta f\end{aligned} \tag{31}$$

where Δf is the disturbance moment caused by road excitation.

Accurately measuring the displacement of the steering pinion and the booster current is difficult due to the disturbing quantities in the state equation, and a robust observer is designed to observe the state quantities.

The EPS system state is reconstructed as equation (32):

$$\begin{aligned}\dot{\lambda}_{\theta_s}&=\lambda_r+l_1(\theta_s-\lambda_{\theta_s})+D_1(\theta_s-\lambda_{\theta_s})\\ \dot{\lambda}_r&=\frac{k_mG}{rm_r}\theta_m+\frac{k_s}{rm_r}\theta_s+D_2(\theta_s-\lambda_{\theta_s})\\ \dot{\lambda}_{\theta_m}&=\lambda_{\theta_s}+l_2(\theta_m-\lambda_{\theta_m})+D_3(\theta_m-\lambda_{\theta_m})\\ \dot{\lambda}_i&=\frac{1}{L}U_s-\frac{k_f}{L}\theta_m+D_4(\theta_m-\lambda_{\theta_m})\end{aligned} \tag{32}$$

where $l_1, l_2, D_1, D_2, D_3, D_4$ are positive real numbers to be designed. $\dot{\lambda}_{\theta_s}$ is the reconstructed value of the steering wheel angle, $\dot{\lambda}_r$ is the reconstructed value of pinion displacement, $\dot{\lambda}_{\theta_m}$ is the reconstructed value of the motor angle, and $\dot{\lambda}_i$ is the reconstructed value of the booster current.

The design observer is as follows:

$$\begin{aligned}\hat{x}_1&=\lambda_{\theta_s}\\ \hat{x}_2&=\lambda_r+l_1(\theta_s-\lambda_{\theta_s})\\ \hat{x}_3&=\lambda_{\theta_m}\\ \hat{x}_4&=\lambda_i+l_2(\theta_m-\lambda_{\theta_m})\end{aligned} \tag{33}$$

where $\hat{x}_i$ is the state estimate.

The estimation error is defined as follows:

$$\tilde{x}_i=x_i-\hat{x}_i \tag{34}$$

Equation (35) can be obtained from equations (31)–(34):

$$\begin{aligned}
&\dot{\hat{x}}_1 = \lambda_r + l_1(\theta_s - \lambda_{\theta_s}) + D_1(\theta_s - \lambda_{\theta_s}) \\
&\dot{\hat{x}}_2 = \frac{k_m G}{rm_r}\lambda_{\theta_m} + \frac{k_s}{rm_r}\theta_s + D_2(\theta_s - \lambda_{\theta_s}) \\
&+l_1(\lambda_r - \hat{x}_2 - D_1 x_1) \\
&\dot{\hat{x}}_3 = \lambda_i + l_2(\theta_m - \lambda_{\theta_m}) + D_3(\theta_m - \lambda_{\theta_m}) \\
&\dot{\hat{x}}_4 = \frac{1}{L}U_s - \frac{k_f}{L}\theta_m + D_4(\theta_m - \lambda_{\theta_m}) \\
&+l_2(\lambda_{\theta_s} - \hat{x}_1 - D_3 x_3)
\end{aligned} \tag{35}$$

Equation (35) is simplified as follows:

$$\begin{aligned}
&\dot{\hat{x}}_1 = \hat{x}_2 + D_1\lambda_{\theta_s} \\
&\dot{\hat{x}}_2 = \frac{k_m G}{rm_r}\lambda_{\theta_m} + \frac{k_s}{rm_r}\theta_s + D_2\lambda_{\theta_s} + l_1\theta_r \\
&\dot{\hat{x}}_3 = \hat{x}_i + D_3\lambda_{\theta_m} \\
&\dot{\hat{x}}_4 = \frac{1}{L}U_s - \frac{k_f}{L}\theta_m + l_2\lambda_{\theta_s} + D_1\lambda_{\theta_m}
\end{aligned} \tag{36}$$

Fig. 4 shows the results of the sliding mode and PID algorithms on the target booster torque tracking. Notably, the sliding mode algorithm can accurately track the target torque, and the corresponding fluctuation is small.

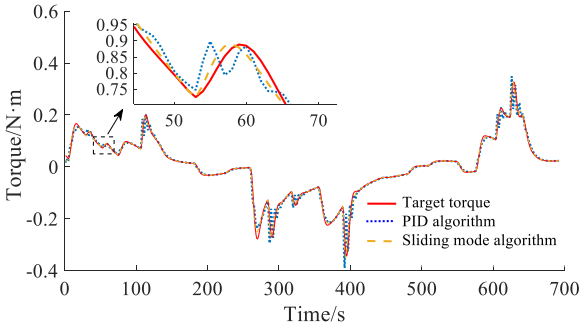

Fig. 4. Target torque tracking curve

3.6 Coefficient of intervention

Lane keeping systems are auxiliary functions that require a balance between driving comfort and safety. These systems will alarm at critical moments and not intervene in safe situations. With the lateral safety distance and driver steering wheel input torque as inputs and the intervention coefficient as output, a fuzzy controller was designed to determine the intervention coefficient. Under small lateral safety distance, large manual force of the driver, and high vehicle speed, the intervention coefficient is small. By contrast, under large lateral safety distance and small manual force input, large lateral safety and driver's manual force and offset in the same direction, and low vehicle speed, the driver is distracted or misuses the driving, the intervention coefficient is large, and the auxiliary control system must make as much input as possible to ensure driving safety while slowing down the driving workload of the driver.

The fundamental domains of the driver's manual force under fuzzy control, lateral safety deviation, and intervention coefficient are [−10, 10], [−5, 5], and [0, 1], respectively. The subsets of the fuzzy variables and intervention coefficients are in seven states: negative big, negative medium, negative small, zero, positive small, positive medium, and positive big. The obtained fuzzy controller input and output affiliation relations are shown in Fig. 5.

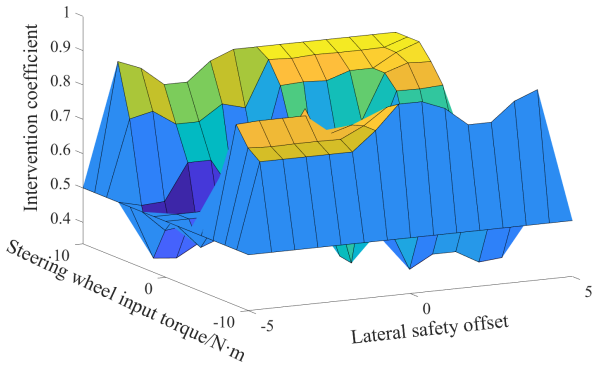

Fig. 5. Intervention coefficient map

4. Result Analysis and Discussion

The simulation parameters involved in the simulation system are shown in Table 1.

Table 1. Main parameters of the system

Parameters	Values	Parameters	Values
M / (Kg)	3021	rp / m	0.0071
Ms / (Kg)	2687	G	16.5
h / (m)	0.488	R / Ω	0.168
Iz / (Kg·m^2)	10437	θs / (N·m·s·rad)	0.261
Isz / (Kg·m^2)	0	Js / (Kg·m^2)	0.0012
Lp / (N.m.s.rad^{-1})	6864	Ks / (N.m.rad)	90
Kc / (V.s.rad^{-1})	0.02	Bs / (N.m.s.rad)	0.261

Simulation test condition: the vehicle speed is 50Km/h. Under four typical road driving conditions, namely, double folium path, double shift path, right turn, and left turn, the steering input of the driver and the steering input under the LKA torque superposition control were simulated. Maintenance control of the established lanes was completed with the performance index parameters of the vehicle position, front-wheel turning angle, and traverse angular velocity.

4.1 Vehicle Front-Wheel Angle Response

Fig. 6 shows the front-wheel angle response curves of the vehicle under four typical road driving conditions. In Fig. 6(a), the front wheel angle of the vehicle decreases by 4.3° after adding LKA control under double folium path conditions. In Fig. 6(b), the front wheel angle of the vehicle decreases by 5° after adding LKA control under double shift path conditions. As presented in Fig. 6(c), the front wheel angle of the vehicle decreases by 9° after adding LKA control under the right turn path condition. In Fig. 6(d), the front wheel angle of the vehicle decreases by 5.3° after adding LKA control under the left turn path condition. The change rate of the wheel angle gradually decreases after adding LKA control, indicating that LKA control can enhance driving smoothness.

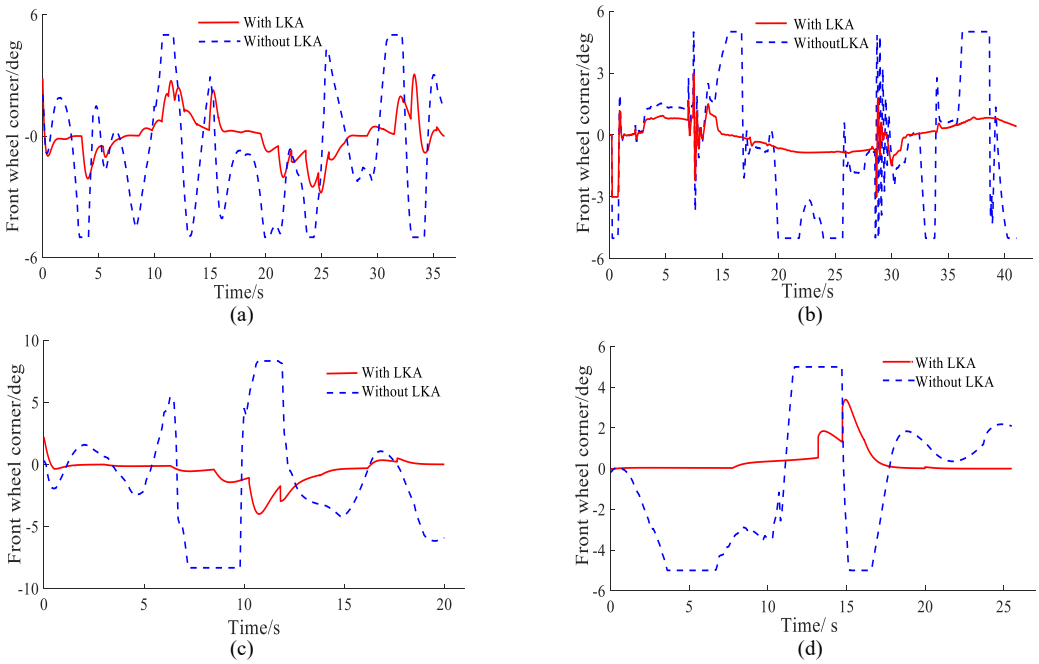

Fig. 6. Front wheel angles of the vehicle under four paths. (a) Front wheel angle under double folium path. (b) Front wheel angle under double shift path. (c) Front wheel angle under right turn path. (d) Front wheel angle under left turn path

4.2 Vehicle yaw Angle Velocity Response

Fig. 7 shows the yaw velocity under four typical road driving conditions. In Fig. 7(a), the yaw velocity of the vehicle decreases by 0.28 rad after adding LKA control under double folium path conditions. In Fig. 7(b), the yaw velocity of the vehicle decreases by 0.52 rad after adding LKA control under double shift path conditions. As shown in Fig. 7(c), the yaw velocity of the vehicle decreases by 0.23 rad after adding LKA control under the right turn path condition. In Fig. 7(d), the yaw velocity of the vehicle decreases by 0.24 rad after adding LKA control under the left turn path condition. The yaw velocity of the vehicle notably decreases after adding LKA control, indicating that the LKA control increases the maneuvering stability of the vehicle.

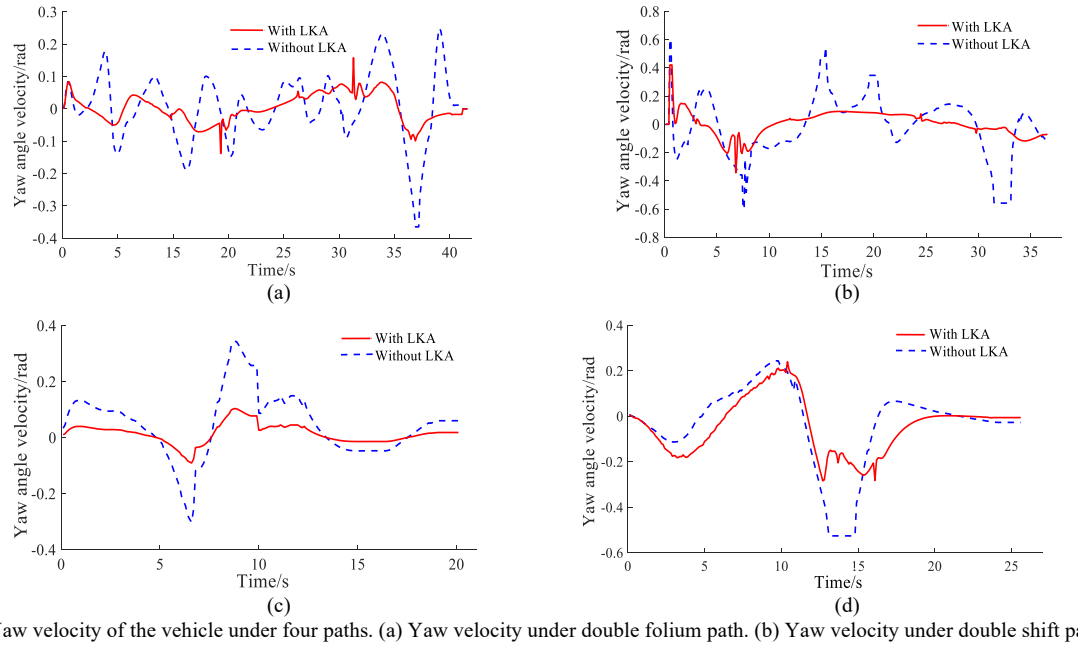

Fig. 7. Yaw velocity of the vehicle under four paths. (a) Yaw velocity under double folium path. (b) Yaw velocity under double shift path. (c) Yaw velocity under right turn path. (d) Yaw velocity under left turn path

4.3 Vehicle Lateral Deflection Response

Fig. 8 shows the comparison curves of vehicle paths under four typical road driving conditions. In Fig. 8(a), the lateral deviation of the vehicle decreases by 2.5 m after adding LKA control under double folium path conditions. In Fig. 8(b), the lateral deviation of the vehicle decreases by 1 m after adding LKA control under double shift path conditions. Fig. 8(c) shows that the lateral deviation of the vehicle decreases by 3.4 m after adding LKA control under the right turn path condition. Fig. 8(d) reveals that the lateral deviation of the vehicle decreases by 1.9 m after adding LKA control under the left turn path condition. The lateral deviation of the vehicle substantially decreases after adding LKA control, indicating that the LKA control can assist in the stable driving of the driver in the intended lane.

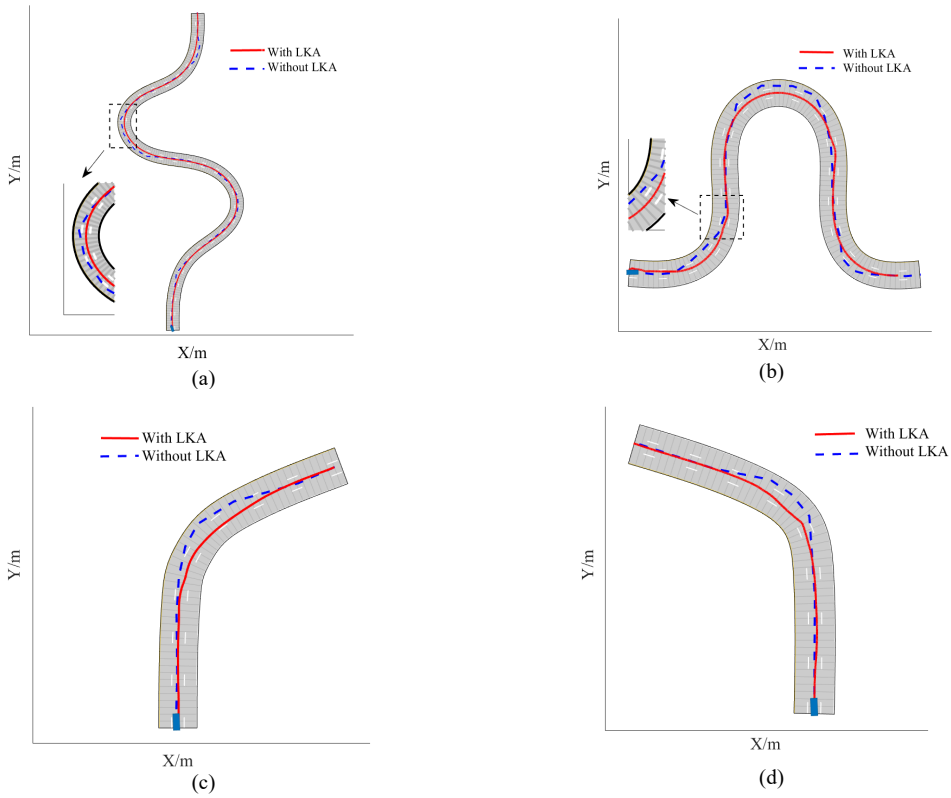

Fig. 8. Vehicle path comparison under four paths. (a) Comparison of vehicle paths under double folium path. (b) Comparison of vehicle paths under double shift path. (c) Comparison of vehicle paths under right turn path. (d) Comparison of vehicle paths under right turn path

5. Conclusions

Starting from EPS system and vehicle modeling, this study used the model predictive control algorithm based on vehicle trajectory and the EPS system control algorithm based on the robust sliding-mode observer to explore the connection between EPS and LKA systems and analyze the assisting torque, front-wheel turning angle, yaw velocity, and lane offset under different road conditions. The following conclusions could be drawn:

(1) The lane keeping control strategy based on electric power steering systems can enhance the maneuvering stability of the vehicle. The front wheel angle and the lateral offset notably decrease. The yaw velocity decreases by a maximum of 0.52 rad, and the wheel angle decreases by a maximum of 9°.

(2) When switching between driver and LKA modes, the designed fuzzy controller-based intervention coefficient can reduce the interference of the LKA system with the driver and realize human-vehicle cooperation.

The EPS and LKA systems were combined in this study to establish control system and intervention coefficient models. The designed LKA strategy can assist in controlling the vehicle back to the original lane when the driver fails to correct the vehicle movement immediately, which provides a study idea for the advanced assisted driving of vehicles. Future studies will combine driving data and LKA system technology due to the lack of support from actual driving data to accurately understand its performance and effectiveness in complex driving scenarios.

Acknowledgements

This work was supported by the special fund for doctoral research (160322001) and scientific research project of Jilin Provincial Department of Education (JJKH20210042KJ) and the education research project of Jilin Province Vocational (2021XHY248).

References

[1] R. Liu, X. Zhao, and X. C. Zhu, "A human-like shared driving strategy in lane-changing scenario using cooperative LPV/MPC," *IEEE Trans. Intell. Transp. Syst.*, vol. 24, no. 9, pp. 9915-9928, Sep. 2023.

[2] C. H. Dai, C. F. Zong, and D. Zhang, "A bargaining game-based human–machine shared driving control authority allocation strategy," *IEEE Transa. Intell. Transp. Syst.*, vol. 24, no. 10, pp. 10572-10586, May. 2023.

[3] K. Li , Z. W. Han , and J. J. Chen , "Fuzzy output feedback coordinated control of lane keeping assistance system," *Trans. Microsyst. Technol.*, vol. 42, no. 12, pp. 95-98+102, Dec. 2023.

[4] M. Marcano , S. Díaz , and J. Pérez , "A review of shared control for automated vehicles: theory and applications," *IEEE Transa. Hum-Mach. Syst.*, vol. 50, no. 6, pp. 475-491, Dec. 2020.

[5] C. F. Zong, C. H. Dai, and D. Zhang , "Human-machine interaction technology of intelligent vehicles: Current development trends and future directions," *China J. Highw. Transp.*, vol. 34, no. 6, pp. 214-237, Apr. 2021.

[6] R. He, X. C. Zhao , and Y. B. Yang , "Man-machine shared driving model using risk-response mechanism of human driver," *J. Jilin Uni. Eng. Technol. Ed.,* vol. 51, no. 3, pp. 799-809, Jul. 2021.

[7] R. He , X. C. Zhao , and J. Q. Wang , "Modeling of driving risk response under human-vehicle-road interaction," *China J. Highw. Transp.*, vol. 33, no. 9, pp. 236-250, Feb. 2020.

[8] Z. H. Yan , K. M. Yang, and Z. Wang, "Intention-based lane changing and lane keeping haptic guidance steering system," *IEEE Transa. Intell. Veh.*,vol. 6 ,no. 4, pp. 622-633, Dec. 2021.

[9] Q. H. Meng , Z. Y. Sun , and Z. Y. Shen , "Homogeneous domination-based lane-keeping control method for intelligent vehicle," *Nonline. Dyn*., vol. 111, no. 7, pp. 6349-6362, Dec. 2022.

[10] Y. Liu, Q. Xu , and H. Guo, "A type-2 fuzzy approach to driver-automation shared driving lane keeping control of semi-autonomous vehicles under imprecise premise variable," *Chin. J. Mechan. Eng.*, vol. 35, no. 1, pp. 1-18, May. 2022.

[11 H. Wang, L. Dai , and Y. Cai, "Salient object detection based on multi-scale contrast," *Neur. Netw.*, vol. 101, pp. 47-56, May. 2018.

[12] C. Y. Liu, F. Chen , and Z. F. Wang , "Design of lane keeping assistance control system based on STM32," *Trans. Microsyst. Technol.*, vol. 41, no. 3, pp. 68-71, May. 2022.

[13] G. B. Shi , H. Q. Zhang , and S. Wang , "Lane-keeping assistance strategy for integrated electric-hydraulic Steering system of commercial vehicles," *China J. Highw. Transp.*, vol. 34, no. 9, pp. 101-110, Sep. 2021.

[14] K. Wöhrl and C. Geisbauer , "Crashed electric vehicle handling and recommendations-state of the art in germany," *Energy.*, vol. 14, no. 4, pp. 1040-1061, Feb. 2021.

[15] H. Q Guo , H. Chen , and J. C. Chen , "Design of lane keeping assistance system based on EPS," *Automob. Technol.*, no. 8, pp. 33-38, Aug.2018.

[16] B. Kővári, B. Pelenczei, and I. G. Knáb, "Beyond trial and error: lane keeping with monte carlo tree search-driven optimization of reinforcement learning," *Electron*., vol. 13, no. 11, pp. 1-18, May. 2024.

[17] Y. C. Huang and L. F. Zhao , "Study on lane keeping performance based on H∞ control of T-S fuzzy model," *J. Hefei Univ. Technol.*, vol. 41, no. 9, pp. 1244-1251, Sep. 2018.

[18] J. H. Kim, S. H. Park, and J. S. Kim, "A deep reinforcement learning strategy for surrounding vehicles-based lane-keeping control," *Sens*., vol. 23, no. 24, pp. 1-17, Dec. 2023.

[19] M. Munadi, B. Radityo, and M. Ariyanto, "Automated guided vehicle (AGV) lane-keeping assist based on computer vision, and fuzzy logic control under varying light intensity," *Resu. Eng*., vol. 21, pp. 101678-101690, Jan. 2024.

[20] H. H. Zheng , Y. Q. Zhang , and Y. X. Bai , "Design of key technologies of lane deviation warning system," *Transd. Microsyst. Technol.*, vol. 38, no. 11, pp. 111-113, Nov. 2019.

[21] H. Alex, T. Reine, and C. Véronique, "A centralized multilayer LPV/H∞ vs decentralized sliding mode control architectures, for the lane keeping and stability of an intelligent vehicle," *IFAC PapOnLine*., vol. 56, no. 2, pp. 4986-4993, Jan. 2023.

[22] Y. Marumo, T. Yokota, and A. Aoki, "Improving stability and lane-keeping performance for multi-articulated vehicles using vector follower control," *Veh. Syst. Dyn.*, vol. 58, no. 12, pp. 1859-1872, Nov. 2019.

[23] S. Chouki, N. T. Anh, and B. M. Amir, "Driver-automation cooperation oriented approach for shared control of lane keeping assist systems," *IEEE Transa. Control. Syst. Technol.*, vol. 27, no. 5, pp. 1962-1978, Sep. 2019.

[24] B. Tang , Y. Yin , and H. B. Jiang , "Lane tracking control of commercial vehicle based on RMPC," *J. Jiangsu Uni. Nat. Sci. Ed.*, vol. 43, no. 3, pp. 256-262, Apr. 2022.

[25] V. Illés and T. Dénes, "Stability analysis of a hierarchical lane-keeping controller with feedback delay," *IFAC PapOnLine*., vol. 55, no. 36, pp. 300-305, Jan. 2022.

[26] K. Zhan , X. Sui , and C. Y. Liu , "Design of lane keeping assistance system for commercial vehicles," *Transd. Microsyst. Technol.*, vol. 41, no. 4, pp. 108-111+116, Apr. 2022.

[27] N. Maryam, A. H. Seddik, and N. N. Thinh, "Robust tube-based LPV-MPC for autonomous lane keeping," *IFAC PapOnLine*., vol. 55, no. 35, pp. 103-108, Jan.2022.

[28] Y. W. Chen , Y. M. Shao , H. B. Shu and X. X. Hao , "Automatic lane keeping control based on safety barrier monitoring," *Automot. Eng.*, vol. 41, no. 7, pp. 771-778, Jul. 2019.

[29] R. N. Tan , W. Wei , and F. Q. Lv , "Design and simulation of lane keeping algorithm based on fuzzy control," *Automob. Appl. Technol.*, no. 15, pp. 101-103, Aug. 2019.